Title: WDR82 mediated H3K4me3 is associated with tumor proliferation and therapeutic efficacy in pediatric high-grade gliomas

Running title: WDR82 mediated H3K4me3 in pediatric gliomas

Nitin Wadhwani,[1] Sonali Nayak,[2] Yufen Wang,[3] Rintaro Hashizume,[4] Chunfa Jie,[5] Barbara Mania-Farnell,[6] Charles David James,[7] Guifa Xi,[2,7] Tadanori Tomita,[2,7]

1. Department of Pathology, Ann & Robert H. Lurie Children's Hospital of Chicago, Northwestern University Feinberg School of Medicine, Chicago, IL 60611 USA
2. Division of Pediatric Neurosurgery, Ann & Robert H. Lurie Children's Hospital of Chicago, Northwestern University Feinberg School of Medicine, Chicago, IL 60611 USA
3. Department of Radio-oncology, Northwestern University Feinberg School of Medicine, Chicago, IL 60611 USA
4. Department of Pediatrics, Northwestern University Feinberg School of Medicine, Chicago, IL 60611 USA
5. Department of Biochemistry and Nutrition, Des Moines University Medicine and Health Sciences, Des Moines, IA 50312 USA
6. Department of Biological Sciences, Purdue University Northwest, Hammond, IN 46323 USA
7. Department of Neurological Surgery, Northwestern University Feinberg School of Medicine, Chicago, IL 60611 USA

Corresponding author
Guifa Xi, MD, PhD
The Department of Neurological Surgery, Northwestern University Feinberg School of Medicine
Address: Simpson Querrey Biomedical Center, Room 6-500
303 Superior Street, Chicago, IL 60611
Phone: (312) 503 4296
Email: xiguifa@yahoo.com

Tadanori Tomita, MD
Division of Pediatric Neurosurgery, Ann & Robert H. Lurie Children's Hospital of Chicago, Northwestern University Feinberg School of Medicine
Address: 225 E Chicago Ave, Box 28
Chicago, IL 60611
Phone: (312) 227 4220
Email: ttomita@luriechildrens.org

Abstract

Pediatric high-grade gliomas (pHGGs) are common malignant brain tumors without effective treatment and poor patient survival. Abnormal posttranslational modification at the histone H3 tail plays critical roles in tumor cell malignancy. We have previously shown that trimethylation of lysine 4 at histone H3 (H3K4me3) plays a significant role in pediatric ependymoma malignancy and is associated with tumor therapeutic sensitivity. Here, we show that H3K4me3 and its methyltransferase WDR82 are elevated in pHGGs. Reduction of H3K4me3 by downregulating WDR82 decreases H3K4me3 promoter occupancy and expression of genes associated with stem cell features, cell proliferation, the cell cycle and DNA damage repair. Reduction of WDR82 mediated H3K4me3 increases the response of pediatric glioma cells to chemotherapy. These findings suggest that WDR82 mediated H3K4me3 is an important determinant of pediatric glioma malignancy and therapeutic response. This highlights the need for a more thorough understanding of the potential of WDR82 as an epigenetic target to increase therapeutic efficacy and improve prognosis for children with malignant gliomas.

Key words

WDR82, epigenetics, proliferation, DNA damage repair, children, high-grade glioma

Introduction

Brain tumors, the most common form of solid tumor in children under the age of 15, are responsible for approximately 20% of all childhood cancers. Five-year survival, following diagnosis and treatment of a primary malignant brain tumor is ~30%. Among pediatric brain tumors, high-grade gliomas (pHGGs), including diffuse intrinsic pontine gliomas (DIPGs), are especially devastating, with an average patient survival of less than 15 months (1). In the last decade, pHGGs have been extensively characterized and remarkable progress has been made at understanding mechanisms associated with the tumors at the molecular level.

Mutations at the histone H3 tail, that change the glycine at residue 34 to either valine or arginine (H3G34V/R) in hemisphere tumors, or a lysine to methionine substitution at residue 27 (H3K27M) in DIPGs (2-6), are common. These mutations remodel chromatin and alter posttranslational histone modifications (PTMs), consequently bringing about abnormal gene expression. Typically, H3G34V/R reduces global H3K36me3 through inhibition of its methyltransferase SETD2 (7). SETD2 is an antagonist of EZH2, a major functional subunit of polycomb repressive complex 2 (PRC2) (8, 9). SETD2 inhibition activates PRC2 and increases H3K27 trimethylation (H3K27me3) (10). H3K27M mutations significantly reduce global H3K27me3 through PRC2 repression (11-13). Strikingly, H3K4me3 is nearly unaffected with either histone gene mutation (14-17). This is unusual, given that H3K4me3 and H3K27me3 are important bivalent histone PTM with respect to the regulation of gene expression in human development and disease (18).

H3K4me3 levels play a role in determining the pathogenesis of various human cancers (19-23), including glial derived brain tumors (24, 25). Additionally, H3K4me3 has prognostic utility for multiple cancers (20, 22, 25). Histone H3 lysine 4 can be mono- (H3K4me1), di- (H3K4me2), or trimethylated (H3K4me3) at the z-amine, or it can be acetylated (H3K4ac). H3K4ac and H3K4me1 are associated with enhancer activity (18, 26, 27). H3K4me2 usually locates to the gene body to stabilize the genome (18, 28). High levels of H3K4me3 are associated with the 5' regions of virtually all active genes, and a strong positive correlation exists between this modification, transcription rates and active polymerase II occupancy (29-33), which is critical for transcriptional activity in a variety of eukaryotic species (30, 33). We have recently shown that high H3K4me3 is associated with poor survival in pediatric ependymoma (25). Its role in pediatric gliomas has not been characterized.

A human SET domain containing 1A/B protein complexes (hSETD1A/B-COMPASS) binds to DNA containing unmethylated CpG motifs and is responsible for trimethylating H3K4 (34). Human SETD1A/B proteins exhibit a large non-overlapping subnuclear distribution, indicating their distinct localization at subsets of target genes (35). These complexes are identical, with the exception of the catalytic component (34, 35). Each complex contains seven units including SETD1A or SETD1B, ASH2, CXXC finger protein 1 (CFP1), DPY30, RBBP5, WDR5, and WDR82 (34-37). WDR82 is an unique subunit of hSETD1A/B (38, 39). WDR82 trimethylates H3K4 through recruitment of hSETD1A/B. WDR82 interacts with hSETD1A/B via an N-terminal RNA recognition motif (RRM) within the latter to mark transcription start sites (TSS) of active genes (33, 38, 40). During early embryonic development, WDR82 is crucial for H3K4me3 at the

promoter of Oct4, whose expression is associated with embryonic stem cells (41). WDR82 is also a component of the PTW/PP1 phosphatase complex, which is involved control of chromatin structure and cell cycle progression during the transition from mitosis to interphase (42). Elevated WDR82 and/or H3K4me3 is associated with therapeutic sensitivity in breast, cervical, ovarian cancers and glioblastomas (43-45). Recent studies show that WDR82 expression is associated therapeutic sensitivity to platinum drugs (43, 46). However, its role in pediatric gliomas has not been investigated.

In this study, H3K4me3 levels and modifiers for this epigenetic mark were mapped using in-house pediatric glioma specimens and via in silico analysis of multiple publicly available databases. WDR82 and H3K4me3 were found to be elevated in pHGGs and associated with chemotherapeutic sensitivity. Reduction of H3K4me3 by downregulation of WDR82 decreased H3K4me3 promoter occupancy and gene expression and increased the response of pediatric glioma cells to chemotherapy. Our data suggest that H3K4me3 status is an important determinant of pediatric glioma malignancy and therapeutic response, and that WDR82, which regulates H3K4me3, is a promising target to increase therapeutic efficacy and improve prognosis for children with malignant gliomas.

Materials and methods

Clinical specimens and immunohistochemistry (IHC). Formalin-fixed, paraffin-embedded (FFPE) pediatric glioma samples were used for immunohistochemical analysis. Samples were collected from patients diagnosed in the Department of Pathology, Ann & Robert H. Lurie Children's Hospital of Chicago (A&RHLCH, Chicago,

IL) under IRB# 2005–12252 (Principle investigator: Dr. Tadanori Tomita). Clinicopathological information is summarized in Supplementary Table 1. All tumor samples were reviewed by a senior pediatric pathologist (N.W), using World Health Organization 2016 criteria for tumor classification. IHC was performed on FFPE slides using antibody against H3K4me3 (Cell signaling Technology, #9727, 1:200) as per manufacturer's instructions. Images were captured on a Leica DMR-HC upright microscope (Leica Microsystem Inc., Buffalo Groove, IL, USA) and analyzed using OpenLab 5.0 software (PerkinElmer, Waltham, MA, USA). H3K4me3 positive staining was graded semi-quantitatively on a five-tier scale: 0□<□10%, 1□+□=10–25%, 2□+□=25–50%, 3□+□=50–75%, 4□+□=□>□75% for positive tumor cell nuclei as described (47).

Cell lines and cultures. Pediatric SJ-GBM2 glioblastoma cells were obtained from the Children's Oncology Group Cell Culture and Xenograft Repository. Pediatric KNS42 cells were purchased from the JCRB (Japanese Cancer Research Resources) cell bank. The human H3K27M DIPG cell line SF8628 was generously provided by Dr. Rintaro Hashizume (Department of Pediatrics, Lurie Children's Hospital of Chicago). All cells were propagated as monolayers in complete medium consisting of Dulbecco's modified Eagle's medium (DMEM,Cat#11965-092) supplemented with 10% fetal bovine serum (FBS, Cat#10082147) from Gibco, at 37 °C with 5% CO_2.

Plasmids. A set of three SMARTvector inducible lentiviral shRNA plasmids with hEF1 promoter and TurboGFP reporter against human WDR82 (Entrez Gene 80335) V3SH11252-229426599 (clone id:V3IHSHEG_9364249, shRNA#1), V3SH11252-

2289952521 (clone id:V3IHSHEG_8890171, shRNA#2), and V3SH11252-230853288 (clone id:V3IHSHEG_10790938, shRNA#3), and non-targeting SMART vector inducible lentiviral with hEF1 promoter and TurboGFP reporter control plasmid were purchased from Horizon Discovery Ltd. (Cambridge, UK). These vectors were amplified and purified as per manufacturer's instructions.

Plasmid transduction. Tumor cells were plated a day before transduction, in 6-well plates at 30-40% confluency, to avoid cell clumps and uneven distribution that can reduce efficacy of viral transduction. Individual wells of confluent cells were treated with packaged lentivirus (100-500ul) and polybrene 4-8 µg/ml, followed by incubation for 6-14h. Cell viability and protein expression were monitored. The transduction process was repeated until an optimal amount of GFP protein was expressed. GFP protein expression was checked after 48-72h using a fluorescent microscope to visualize the fluorescent tag present in the construct. Cells were than selected with antibiotics. In cases where the construct needed a substrate such as doxycycline (Dox) for induction, Dox was added and protein expression was monitored after 24h, 48h and 72h.

Total, Nuclear and Histone Protein Extraction and Immunoblotting. Total proteins were extracted with Tissue Extraction Buffer I (Life Technologies, cat# FNN0071) with proteinase (Cell Signaling Technology, Beverly, MA, USA), phosphatase (Sigma) inhibitor cocktails and phenylmethylsulphonyl fluoride (PMSF, Roche). Total histone was extracted using histone extraction kit (ab113476, Abcam) as per manufacturer's instructions. Protein concentrations were quantified with the BCA Protein Assay Kit (Thermo Fisher Scientific Inc.) using Nanodrop ND-2000 (Thermo Fisher Scientific Inc.).

Equal amounts of cell lysate were resolved by sodium dodecyl sulfate–polyacrylamide gel electrophoresis and transferred to nitrocellulose membranes (Bio-Rad, Hercules, CA, USA). Blocking was performed for 60 min with 5% nonfat dry milk in Tris-buffered saline and Tween 20, followed by blotting with primary antibodies overnight at 4 °C. Primary antibodies include polyclonal anti-rabbit WDR82 (Cat#99715, 1:1000), H3K4me3 (Cat#9727, 1:1000) and H3 (Cat#9715, 1:2500) from Cell Signaling Technology; hSETD1A from Bethyl Laboratories (Cat#A300-289A, 1:1000); β-actin (ab8227,1:3000) from Abcam; rabbit polyclonal anti-GAPDH (sc-25,778, 1:2000) from Santa Cruz Biotechnology. After washing with Tris-buffered saline and Tween 20, membranes were incubated for 1h at room temperature with horseradish peroxidase (HRP) conjugated donkey anti-rabbit antibody (sc-2305, 1:5000), and signal was detected with enhanced chemiluminescence substrate (Bio-Rad Laboratories).

In silico public dataset analysis. Two expression profiling datasets (GSE50161, GSE73038) were downloaded from the GEO database at the NCBI. Original gene expression profiles were obtained from these two datasets. Expression of individual genes was identified with GEO2R. Adult low- and high-grade glioma data in TCGA were processed with the Gliovis online portal (http://gliovis.bioinfo.cnio.es/). Data was further analyzed with Graphpad Prism 9.0 for gene expression, gene expression correlation and survival analysis (GraphPad Software, Inc. La Jolla, CA, USA).

RNA-seq. Total RNA was prepared using the RNeasy Mini Kit (Qiagen, Cat#74106) as per manufacturer's instructions. Stranded mRNA-seq was conducted in the Northwestern University Sequence (NUseq) Core Facility. Briefly, total RNA samples

were checked for quality using RINs generated from Agilent Bioanalyzer 2100 (Agilent Technologies, Santa Clara, CA). RNA quantity was determined with the Qubit fluorometer (Qubit 2.0, Thermofisher, Waltham, MA). The Illumina TruSeq Stranded mRNA Library Preparation Kit (Cat#20020595, Illumina, Inc., San Diego, CA) was used to prepare sequencing libraries from 1 mg of high-quality RNA samples (RIN=10). The Kit procedure was performed without modification. The procedure includes mRNA purification and fragmentation, cDNA synthesis, 3' end adenylation, Illumina adapter ligation, library PCR amplification and validation. Illumina HiSeq 4000 sequencer was used to sequence the libraries with the production of single-end, 50 bp reads at the depth of 30-40 M reads per sample. The quality of reads, in FASTQ format, was evaluated using FastQC. Adapters were trimmed and reads of poor quality or aligning to rRNA sequences were filtered. The cleaned reads were aligned to the *H. sapiens* genome using STAR (48). Read counts for each gene were calculated using HTseq-count (49), in conjunction with a gene annotation file for hg38 obtained from UCSC (http://genome.ucsc.edu). Differential expression was determined using DESeq2 (50). The cutoff for determining genes, which show significant differential expression, was an FDR-adjusted p-value less than 0.05.

ChIP-seq. Fragmental DNA for ChIP-seq was prepared using SimpleChIP® Plus Enzymatic Chromatin IP Kit (Magnetic Beads) (Cell Signaling Technologies, Cat#9005) per manufacturer's instructions. ChIP-seq was conducted in the NUseq Core Facility. Briefly, ChIP and input DNA samples were checked for quality and quantity using Qubit and Agilent Bioanalyzer (Agilent Technologies, Santa Clara, CA). After passing quality control), the Illumina TruSeq ChIP Sample Preparation Kit (IP-202-1012 & IP-202-1024, Illumina, Inc., San Diego, CA) was used to

prepare sequencing libraries from 5-10 ng of ChIP and input DNA. This procedure includes end repair, 3' end adenylation, Illumina adapter ligation, library PCR amplification and validation. Illumina HiSeq 4000 sequencer was used to sequence the libraries with the production of single-end, 50 bp reads at the depth of 30-40 M reads per sample. After sequencing, the quality of reads, in FASTQ format, will be evaluated using FastQC. Adapters will be trimmed; reads of poor quality will be filtered. The cleaned reads will be aligned to the *H. sapiens* genome (hg38) using Bowtie (51). Peak calling and differential peak analysis will be performed using HOMER (http://homer.ucsd.edu/homer/index.html).

Cell proliferation assay. SJ-GBM2 and SF8628 cells were used to determine if reducing WDR82 through inducible knockdown affected cell viability 1×10^4 cells/100µl were plated in 96-well plates with complete cell culture medium with or without Dox (2µg/ml), and subjected to 3-(4, 5-dimethylthiazol-2-yl)-5-(3-carboxymethoxyphenyl)-2-(4-sulfophenyl)-2H-tetrazolium (MTS, Promega) assay.

Clonogenic survival assay. Pediatric high-grade glioma KNS42 cells were seeded into 6-well tissue culture plates and allowed to adhere. Attached cells were treated with or without doxycycline (SKU#D9891-10G, Sigma-Aldrich) at 2µg/ml. Cells were incubated with doxycycline for 2 weeks, at which time colonies were counted following staining with methylene blue (0.66% solution in 95% ethanol). Plating efficiencies were calculated as the ratio of the number of colonies formed to the number of cells seeded.

In vivo studies. 6-8 week old athymic nude mice were purchased from Taconic. All mice were housed under aseptic conditions, which included filtered air and sterilized food, water, bedding, and cages. The Institutional Animal Care and Use Committee (IACUC) approved all animal protocols. SJ-GBM2 (1 x 10^5) or KNS42 (2 x10^5) cells, transduced with sh-WDR82 vectors, or non-transduced controls, were implanted into the right striatum. Mice were given 1% sucrose or 1% sucrose + 2mg/ml doxycycline in their drinking water (52), which was replaced every 2-3 days. Animals were monitored daily and body weight was measured every 2-3 days. Mice were euthanized with CO2 asphyxiation followed by cervical dislocation when they became moribund (e.g. >20% weight loss, neurologic symptoms, or evidence of pain/distress). Brains were harvested and fixed with 10% paraformaldehyde in PBS overnight and switched to PBS prior to embedding. The tissue was sectioned onto slides and stained with H&E. Tissue preparation was done at the Mouse Histology and Phenotyping Laboratory (MHPL), Northwestern University Feinberg School of Medicine.

Statistical analysis. Cell proliferation results were read on a Synergy 2 Microplate Reader (BioTek Instruments Inc., VT, USA). Cell survival is presented as a percentage of viable cells compared to the viable cell number in the corresponding control, with the control set as 100%. *P* values were calculated using two-way ANOVA, with $P < .05$ considered significant. Statistical tests were 2-sided. Kaplan-Meier and t-tests were performed to compare survival between groups. Graph generation and statistical analyses were performed with GraphPad Prism 9 software (GraphPad Software, Inc. La Jolla, CA, USA).

RESULTS

H3K4me3 Levels Increase with histopathological malignancy in pediatric gliomas. To investigate whether a correlation exists between clinicopathologic variables and H3K4me3, forty-six pediatric low-grade glioma (WHO grades I&II) and ten pediatric high-grade glioma (WHO grades III&IV) FFPE specimens were IHC stained for H3K4me3 (Supplementary Table 1). H3K4me3 was predominantly observed in cell nuclei with the frequency of immunopositive cells ranging from 0% to 100%. Patient gender and tumor location are not associated with H3K4me3 levels. Patient age and WHO grade positively correlated with H3K4me3 levels. IHC results showed H3K4me3 significantly increased in pHGGs, relative to pLGGs (Figure 1 A and B). Multivariate Cox proportional hazards analysis showed that progression free survival of patients with high levels of H3K4me3 (IHC score ≥3) was significantly shorter relative to patients with low levels of H3K4me3 (IHC score ≤2) (Figure 1C). Western blots of protein extracts from tissue samples confirmed higher levels of H3K4me3 in pHGGs vs. pLGGs (Figure 1D). These results indicate that H3K4me3 IHC staining is an accurate predictor of pediatric glioma malignancy especially in pHGGs, irrespective of the presence or absence of histone H3 mutations.

WDR82 plays a distinct role in the tumor biology of pediatric glioma. H3K4 is reversibly modified by methyltransferases and demethylases. To identify key modifier(s) of H3K4 in pHGGs, gene expression profiling with microarray analysis revealed that WDR82, among all H3K4 modifiers, is differentially expressed at significant levels and correlates with WHO grade malignancy, regardless of histone mutation subtypes (Figure 2A and B). These results are supported by in silico analysis of a glioma gene

expression profiling dataset (GSE50161, Supplementary Figure 1A). Geneontology function analysis indicates that WDR82 expression is related to multiple biological processes, molecular function and cellular signaling pathways (Figure 2C), The level of WDR82 shows an inverse correlation with patient survival (Figure 2D). Interestingly, in silico analysis results from The Cancer Genome Atlas (TCGA) shows that WDR82 does not correlate with WHO grade malignancy and survival in adult gliomas (Figure 2E and F). In combination, these results indicate that WDR82 expression is specifically relevant to the tumor biology of pHGGs.

Altered gene expression following WDR82 inducible knockdown. We have shown that WDR82 is highly expressed in pHGGs vs. pLGGs. To investigate the role of WDR82 in pHGGs, pHGG cell lines SJ-GBM2, SF8628 and KNS42 were transduced with SMARTvector inducible lentiviral shRNA targeting WDR82 (shRNA#1 and shRNA#2) or non-targeting control vector (Figure 3A). The results show that GFP is expressed (green fluorescence) at day 5 in transduced cells following Dox (2µg/ml) treatment, whereas untreated cells show no fluorescence (Figure 3B). We further checked WDR82 expression in these cells by real-time PCR (Figure 3C) and western blot (Figure 3D). WDR82 and H3K4me3 levels significantly decreased.

To identify altered gene expression, with WDR82 knockdown, total RNA was extracted from transduced cells in the absence or presence of Dox (2µg/ml) at day 5 and sequenced (RNA-seq and ChIP-seq with H3K4me3 antibody immunoprecipitation). The RNA-seq results from SJ-GBM2 cells indicate that 129 genes were differentially (cutoff: 1.5 times) expressed in cells transduced with shRNA#1 and shRNA#2, in comparison to

non-significant gene expression changes with non-target shRNA (shNT) controls in the presence or absence of Dox (Figure 4 A-C). We further analyzed the function of these genes using the Gene Ontology online portal (http://geneontology.org/). The results showed that reducing WDR82 significantly decreases expression of genes associated with mitosis, proliferation, and DNA repair (Figure 4D). ChIP-seq results indicate that LIN9 and NUP43 promoter H3K4me3 levels decreased in SJ-GBM2 cells transduced with inducible shRNA#2 against WDR82 following Dox induction (Figure 4E).

WDR82 mediated H3K4me3 is associated with mitotic and cell cycle related gene regulation. To investigate if changes in gene expression link to WDR82 mediated H3K4me3 alteration at their promoters, representative genes were selected. Correlation between gene expression and WDR82 was plotted using RNA-seq results from pediatric glioma tissue specimens. Promoter H3K4me3 levels were mapped using ChIP-seq results SJ-GBM2 cells treated with Dox inducible shRNA vector against WDR82 (shRNA#2), in the absence and presence of Dox. The representative results showed WDR82 did not correlate with expression of NUP62 and FBOX10, genes for which levels increased in pediatric glioma tissue specimens (Figure 5A). Additionally, H3K4me3 at their promoters was unaltered (Figure 5B). In the group of genes with decreased expression, there was correlation with WDR82 in pediatric glioma tissue specimens, representative results are shown for NUP43 and PKYMT1 (Figure 5C). Furthermore, H3K4me3 promoter levels were undetectable in SJ-GBM2 cells treated with inducible shRNA#2 against WDR82, following Dox or non-Dox treatment (Figure 5D).

WDR82 knockdown decreases in vitro cell viability and DNA damage repair in pHGG cells. To investigate whether WDR82 levels affect pHGG cell growth, equal numbers of cells were plated in 96-well plates in the absence and presence of Dox (2µg/ml), with relative cell numbers compared at 0~7 days by MTS assay. OD values for Dox treated groups were normalized based on the values of corresponding untreated cells. Inducible knockdown of WDR82, following Dox treatment, significantly suppresses cell growth in SJ-GBM2 and SF8628 cells (Figure 6A). Inducible knockdown of WDR82 also affects pHGG KNS42 cell proliferation, as indicated by colony formation assay (Figure 6 B and C). KNS42 cells were plated (125, 250, 500 cells) in 6-well plates and cultured in the absence or presence of Dox (2µg/ml) for two weeks prior to counting colonies stained with methylene blue (0.66% solution in 95% ethanol).

CDK2 is associated with CCND1 which regulates cell proliferation, the cell cycle and DNA damage repair in childhood cancer through regulation of Rb (53). CDK2 decreased in SJ-GBM2 cells treated with inducible shRNA#2 against WDR82, following Dox vs. non-Dox treatment (Figure 4C). We hypothesized that CDK2 and CCND1 are regulated by WDR82 mediation of promoter H3K4me3. To verify this hypothesis, CDK2, CCND1 and WDR82 expression were examined in pediatric gliomas. A significant correlation was identified (Figure 6D). ChIPseq results showed that at the promoters of these two genes, H3K4me3 decreased in SJ-GBM2 cells, treated with inducible shRNA#2 against WDR82, following Dox vs. non-Dox treatment (Figure 6E). These results indicate that

WDR82 mediated H3K4me3 alteration is associated with cell proliferation, the cell cycle and DNA damage repair (Figure 6F).

WDR82 knockdown increases therapeutic sensitivity against DNA-damaging agents and radiation sensitivity. Increased WDR82 expression is associated with tumor malignancy grade (Figure 2A). Recent studies have shown that overexpression of WDR82 promotes high H3K4me3 in tumors following chemotherapy (43, 46). Our RNA-seq results from SJ-GBM2 cells indicate that reduction of WDR82 impairs DNA repair and increases apoptosis. We hypothesized that reduction of WDR82 could increase sensitivity to chemotherapeutic agents which break double stranded DNA, and to radiation. To verify this hypothesis, the effect of inducible WDR82 knockdown was investigated in SJ-GBM2 and SF8628 in cells treated with cisplatin (CDDP), a first-line clinical drug for treating pHGG patients. Inducible WDR82 knockdown by Dox increased sensitivity to CDDP (Supplementary Figure 2A). We also tested whether inducible WDR82 knockdown by Dox increases cell response to radiation following a clonogenic assay protocol as described (54). WDR82 reduction increased radiation sensitivity in KNS42 cells, as indicated by comparison of colony numbers (Supplementary Figure 2B) and calculating the dose of enhancement factors (DEFs) at 10% survival (Supplementary Figure 2C).

WDR82 knockdown decreases in vivo pHGG tumor growth and extends survival of pHGG tumor bearing mice. WDR82 contributes to tumorigenesis, malignant phenotype and tumor proliferation of multiple human cancers (55, 56). To investigate if

WDR82 and H3K4me3 correlate to proliferation in pediatric glioma specimens, PCNA, MIK67, WDR82 and H3K4me3 expression was examined. WDR82 correlated with PCNA and MIK67 (Figure 7A) and Ki67 associated with H3K4me3 (Figure 7B). To investigate if WDR82 knockdown decreases pHGG tumor growth in vivo, 1 x 10^5 cells (SJ-GBM2 transduced with shNT and WDR82 shRNA#2) were inoculated intracranially into the right striatum of 6-8 week old athymic nude mice. Mouse housing and tissue processing as described under *in vivo* studies. Tumor size and mitotic cells are not significantly different in non-targeted shRNA (shNT) groups with or without Dox. In contrast, tumor size is smaller and there are less mitotic cells in the group treated with Dox, as indicated by comparing results from animals given Dox vs. 1% sucrose, (Figure 7C, D and E). The results also showed survival was significantly extended in mice in the WDR82 shRNA#2 + Dox group (Figure 7F). These results indicate that suppression of WDR82 decreases cell growth and extends tumor bearing animal survival.

Discussion

In a previous study we established that H3K4me3 is associated with WHO grade malignancy in pediatric ependymomas (25). In this work we found that H3K4me3 is also associated with WHO grade in pediatric gliomas, with higher levels of H3K4me3 in HGGs vs. LGGs (Figure 1A). Patients with higher tumor levels of H3K4me3 had a shorter progression free survival (Figure 1C). Furthermore, WDR82, an H3K4me3 methyltransferase, is elevated in pHGGs vs. LGGs, which is inversely correlated with clinical prognosis (Figure 2). Furthermore, we also found that WDR82 meditated H3K4me3 alters gene expression related to a variety of biological functions including

stem cell features, cell proliferation, the cell cycle and DNA damage repair. The results highlight the necessity of a thorough understanding of the biological roles of WDR82 and H3K4me3 in pediatric glioma. This knowledge will establish if WDR82 and H3K4me3 are potential epigenetic targets to suppress tumor progression, increase therapeutic efficacy, and improve outcomes for children with malignant gliomas.

The discovery of recurrent histone mutations in children with pHGGs in the last decade revealed that PTMs on histone tails are one of the milestone changes whose role must be elucidated in cancer research. In pediatric gliomas, H3G34V/R in hemisphere tumors and H3K27M in midline gliomas including DIPG are common histone mutations (2-6). These mutations crosstalk with other histone modifications and bring about abnormal gene expression involved in pediatric malignant glioma tumorigenesis. Recently, H3K36me2 and H4K16Ac were discovered to be novel epigenetic signatures of DIPG (57). H3K4me3, an important histone mark for developmental neurogenesis, was relatively unaffected regardless of these mutations as shown with western blot analysis (14-17). However, ChIP-seq analysis to investigate promoter H3K27me3 and H3K4me3 in wild-type (WT) and H3K27M NSCs and DIPGs, showed elevated promoter H3K4me3 in H3K27M induced genes such as Lin28b, Igf2bp2, Plag1, Pbx3, Eya1, etc. These genes regulate neuroprogenitor cell proliferation and differentiation and are associated with DIPG oncogenic signature (58). Another study used ChIPseq to map promoter H3K27me3 and H3K4me3 was examined in DIPGs with and without H3K27M knockdown, promoter H3K4me3 changed in differentially expressed genes, with increased levels in K27M-induced upregulated genes, for example RORB and VIM (16).

H3K4me3 is activated in pHGGs with H3.3G34R/V mutation in comparison with WT tumors (59). In this study, we determined that H3K4me3 is elevated in pHGGs vs. pLGGs (Figure 1 and Supplementary Table 1), and its reduction via decreasing WDR82 alters the expression of genes involved in cell proliferation, the cell cycle and DNA damage repair. Altogether, these findings suggest H3K4me3 impacts pHGGs, which merits further investigation.

Among the six methyltransferases for H3K4me3, SETD1A is associated with WHO malignancy in pediatric gliomas (Figure 1D, Supplementary Figure 1A). Investigation of its subunits WDR82, ASH2L DPY30 CXXC1, RBBP5 and WDR5, showed WDR82 and WDR5 significantly associated with WHO grade malignancy in pediatric gliomas (Figure 1C, Supplementary Figure 1C and Figure 2). WDR5 is also associated with malignancy in adult gliomas (60-64). WDR82 is the sole subunit in SETD1A-COMPASS, specifically associated with pediatric glioma WHO grade malignancy (Figure 2A) and patient survival (Figure 2D), regardless of histone mutation status Supplementary Figure 3), it is not correlated with adult glioma WHO grade malignancy or patient survival (Figure 2E and F). Due to this specificity for pediatric gliomas, WDR82 mediated H3K4me3 is the focus of this study.

WDR82 activity is a key factor in maintaining embryonic (34), and cancer stem cells (42, 43). In this work sphere formation was impaired in shWDR82 transduced cells following Dox treatment, in comparison to non-Dox treatment and shNT groups, respectively (Supplementary Figure 4 A and B). Results from in silico analysis of dataset GSE50161

showed a positive correlation between WDR82 and expression of SOX2, (Supplementary Figure 4C), a glioma stem cell determinant (65-67), and one of the genes decreased in Figure 2B. ChIP-seq results from SJ-GBM2 cells show that WDR82 knockdown causes promoter H3K4me3 reduction at the SOX2 gene (Supplementary Figure 4D). These results are consistent with previous findings (41, 68) and provide further confirmation that WDR82 mediated H3K4me3 is associated with stem cell characteristics.

In the present study, WDR82 mediated H3K4me3 alters gene expression of NUP43 (69, 70), LIN9 (71-73), PKMYT1 (74, 75), CDK2 (76, 77), LOX (78, 79) and NUP62 (80, 81), genes associated with mitosis, the cell cycle and DNA damage repair in pHGGs (Figures 4, 5 and 6). WDR82 association with these genes is a novel finding, however, the results are consistent with discoveries in embryonic stem cells and various human cancer cells. For instance, WDR82 mediated H3K4me3 is responsible for facilitating M-phase progression in mixed lineage leukemia. WDR82 knockdown increases mitotic cells (82)**.** WDR82 modulates cell cycle progression through regulation of the B-cell translocation gene 2 (BTG2). Depletion of WDR82 induces expression of BTG2, an anti-proliferative protein (83, 84). WDR82 mediated H3K4me3 reduction induces apoptosis in embryo stem cells (41). WDR82 and/or H3K4me3 are associated with chemotherapeutic sensitivity in breast, cervical and ovarian cancers, and adult glioblastoma cells (43-45). WDR82 is an important binding partner with TOX4 in HeLa cells following cisplatin treatment (43, 46). Our results, showing inducible reduction of WDR82 sensitizes pediatric glioma cell response to cisplatin and radiation therapy

(Supplementary Figure 2), are also in line with alterations in gene expression observed in this work. Taken together these findings demonstrate that WDR82 regulates gene expression associated with mitosis, proliferation and the cell cycle, as well as apoptosis and chemotherapeutic response in pHGGs, and thus may be a potential therapeutic target.

In summary, H3K4me3 and WDR82 are elevated in pHGGs vs pLGGs. WDR82 mediated H3K4me3 is associated with expression of genes involved in regulating stem cell features, cell mitosis and proliferation, the cell cycle and DNA damage repair. Reduction of WDR82 increased the response of pediatric glioma cells to chemotherapy. Inducible reduction of WDR82 decreases pHGG tumor cell growth in vivo and extends animal survival. These findings suggest that WDR82 mediated H3K4me3 is a significant factor in pediatric glioma, and further investigation of WDR82 as a promising epigenetic therapeutic target for pHGG is warranted.

Authors' contributions

Conception and design: GX, TT. Development of methodology: BM-F, GX, CDJ. Acquisition of data (Clinic database and pathology reviewing, immunofluorescence, real-time PCR, western blot and flow cytometry etc.): NW, SN, YW, LW, GX and TT. Analysis and interpretation of data (e.g., statistical analysis, biostatistics, computational analysis): CJ, GX, YL, TT. Writing, review, and/or revision of the manuscript: BM-F, GX, CJ, TT. Administrative, technical, or material support (i.e., reporting or organizing data, constructing databases): RH, GX, TT. Study supervision: CDJ, TT. All authors read and approved the final manuscript.

Competing interests

The authors declare no competing interest.

Acknowledgements

The authors would like to thank GETiN Core (Gene Editing, Transduction and Nanotechnology Core), SBDRC (Skin Biology & Disease Resource-Based Center) at Northwestern University for processing lentivirus stocks and cell transductions and the staff of the NUseq Core Facility for technique assistance and guidance of RNA- and ChIP-sequencing. The authors would also like to thank the department of histology and pathology at A&RLCH for preparation of pathology slides.

This work was supported, in part, by the National Cancer Institute SPORE grant (P50CA221747-01A1) Career Enhancement Award; St. Baldrick Foundation and the Rory David Deutsch Foundation, the Surgical Neuro-Oncology Research Fund of Ann & Robert H Lurie Children's Hospital (A&RLCH) of Chicago, and the Dr. Ralph and Marian C. Falk Medical Research Trust.

References

1. Ostrom QT, Egan KM, Nabors LB, Gerke T, Thompson RC, Olson JJ, et al. Glioma risk associated with extent of estimated European genetic ancestry in African Americans and Hispanics. *Int J Cancer.* 2020;146(3):739-48.
2. Sturm D, Witt H, Hovestadt V, Khuong-Quang DA, Jones DT, Konermann C, et al. Hotspot mutations in H3F3A and IDH1 define distinct epigenetic and biological subgroups of glioblastoma. *Cancer cell.* 2012;22(4):425-37.

3. Schwartzentruber J, Korshunov A, Liu XY, Jones DT, Pfaff E, Jacob K, et al. Driver mutations in histone H3.3 and chromatin remodelling genes in paediatric glioblastoma. *Nature.* 2012;482(7384):226-31.

4. Khuong-Quang DA, Buczkowicz P, Rakopoulos P, Liu XY, Fontebasso AM, Bouffet E, et al. K27M mutation in histone H3.3 defines clinically and biologically distinct subgroups of pediatric diffuse intrinsic pontine gliomas. *Acta Neuropathol.* 2012;124(3):439-47.

5. Fontebasso AM, Gayden T, Nikbakht H, Neirinck M, Papillon-Cavanagh S, Majewski J, et al. Epigenetic dysregulation: a novel pathway of oncogenesis in pediatric brain tumors. *Acta Neuropathol.* 2014;128(5):615-27.

6. Wu G, Broniscer A, McEachron TA, Lu C, Paugh BS, Becksfort J, et al. Somatic histone H3 alterations in pediatric diffuse intrinsic pontine gliomas and non-brainstem glioblastomas. *Nat Genet.* 2012;44(3):251-3.

7. Fang J, Huang Y, Mao G, Yang S, Rennert G, Gu L, et al. Cancer-driving H3G34V/R/D mutations block H3K36 methylation and H3K36me3-MutSα interaction. *Proc Natl Acad Sci U S A.* 2018;115(38):9598-603.

8. Diehl KL, Ge EJ, Weinberg DN, Jani KS, Allis CD, and Muir TW. PRC2 engages a bivalent H3K27M-H3K27me3 dinucleosome inhibitor. *Proc Natl Acad Sci U S A.* 2019;116(44):22152-7.

9. Jani KS, Jain SU, Ge EJ, Diehl KL, Lundgren SM, Muller MM, et al. Histone H3 tail binds a unique sensing pocket in EZH2 to activate the PRC2 methyltransferase. *Proc Natl Acad Sci U S A.* 2019;116(17):8295-300.

10. Shi L, Shi J, Shi X, Li W, and Wen H. Histone H3.3 G34 Mutations Alter Histone H3K36 and H3K27 Methylation In Cis. *J Mol Biol.* 2018;430(11):1562-5.

11. Piunti A, Smith ER, Morgan MAJ, Ugarenko M, Khaltyan N, Helmin KA, et al. CATACOMB: An endogenous inducible gene that antagonizes H3K27 methylation

activity of Polycomb repressive complex 2 via an H3K27M-like mechanism. *Science advances.* 2019;5(7):eaax2887.

12. Lee CH, Yu JR, Granat J, Saldana-Meyer R, Andrade J, LeRoy G, et al. Automethylation of PRC2 promotes H3K27 methylation and is impaired in H3K27M pediatric glioma. *Genes Dev.* 2019; 33(19-20).
13. Harutyunyan AS, Krug B, Chen H, Papillon-Cavanagh S, Zeinieh M, De Jay N, et al. H3K27M induces defective chromatin spread of PRC2-mediated repressive H3K27me2/me3 and is essential for glioma tumorigenesis. *Nat Commun.* 2019;10(1):1262.
14. Lewis PW, Muller MM, Koletsky MS, Cordero F, Lin S, Banaszynski LA, et al. Inhibition of PRC2 activity by a gain-of-function H3 mutation found in pediatric glioblastoma. *Science.* 2013;340(6134):857-61.
15. Chan KM, Fang D, Gan H, Hashizume R, Yu C, Schroeder M, et al. The histone H3.3K27M mutation in pediatric glioma reprograms H3K27 methylation and gene expression. *Genes Dev.* 2013;27(9):985-90.
16. Silveira AB, Kasper LH, Fan Y, Jin H, Wu G, Shaw TI, et al. H3.3 K27M depletion increases differentiation and extends latency of diffuse intrinsic pontine glioma growth in vivo. *Acta Neuropathol.* 2019; 137(4):637-55.
17. Lu C, Jain SU, Hoelper D, Bechet D, Molden RC, Ran L, et al. Histone H3K36 mutations promote sarcomagenesis through altered histone methylation landscape. *Science.* 2016;352(6287):844-9.
18. Gu B, and Lee MG. Histone H3 lysine 4 methyltransferases and demethylases in self-renewal and differentiation of stem cells. *Cell & bioscience.* 2013;3(1):39.
19. Zhao F, Chen Y, Zeng L, Li R, Zeng R, Wen L, et al. Role of triptolide in cell proliferation, cell cycle arrest, apoptosis and histone methylation in multiple myeloma U266 cells. *Eur J Pharmacol.* 2010;646(1-3):1-11.

20. He C, Xu J, Zhang J, Xie D, Ye H, Xiao Z, et al. High expression of trimethylated histone H3 lysine 4 is associated with poor prognosis in hepatocellular carcinoma. *Hum Pathol.* 2012;43(9):1425-35.

21. Ke XS, Qu Y, Rostad K, Li WC, Lin B, Halvorsen OJ, et al. Genome-wide profiling of histone h3 lysine 4 and lysine 27 trimethylation reveals an epigenetic signature in prostate carcinogenesis. *PloS one.* 2009;4(3):e4687.

22. Seligson DB, Horvath S, Shi T, Yu H, Tze S, Grunstein M, et al. Global histone modification patterns predict risk of prostate cancer recurrence. *Nature.* 2005;435(7046):1262-6.

23. Neilsen BK, Chakraborty B, McCall JL, Frodyma DE, Sleightholm RL, Fisher KW, et al. WDR5 supports colon cancer cells by promoting methylation of H3K4 and suppressing DNA damage. *BMC cancer.* 2018;18(1):673.

24. Sandstrom RS, Foret MR, Grow DA, Haugen E, Rhodes CT, Cardona AE, et al. Epigenetic regulation by chromatin activation mark H3K4me3 in primate progenitor cells within adult neurogenic niche. *Sci Rep.* 2014;4:5371.

25. Lewis R, Li YD, Hoffman L, Hashizume R, Gravohac G, Rice G, et al. Global Reduction of H3K4me3 Improves Chemotherapeutic Efficacy for Pediatric Ependymomas. *Neoplasia (New York, NY).* 2019;21(6):505-15.

26. Bae S, and Lesch BJ. H3K4me1 Distribution Predicts Transcription State and Poising at Promoters. *Frontiers in cell and developmental biology.* 2020;8:289.

27. Local A, Huang H, Albuquerque CP, Singh N, Lee AY, Wang W, et al. Identification of H3K4me1-associated proteins at mammalian enhancers. *Nat Genet.* 2018;50(1):73-82.

28. Zhang J, Parvin J, and Huang K. Redistribution of H3K4me2 on neural tissue specific genes during mouse brain development. *BMC genomics.* 2012;13 Suppl 8:S5.

29. Shilatifard A. The COMPASS family of histone H3K4 methylases: mechanisms of regulation in development and disease pathogenesis. *Annu Rev Biochem.* 2012;81:65-95.

30. Schneider R, Bannister AJ, Myers FA, Thorne AW, Crane-Robinson C, and Kouzarides T. Histone H3 lysine 4 methylation patterns in higher eukaryotic genes. *Nature cell biology.* 2004;6(1):73-7.

31. Bernstein BE, Kamal M, Lindblad-Toh K, Bekiranov S, Bailey DK, Huebert DJ, et al. Genomic maps and comparative analysis of histone modifications in human and mouse. *Cell.* 2005;120(2):169-81.

32. Bernstein BE, Mikkelsen TS, Xie X, Kamal M, Huebert DJ, Cuff J, et al. A Bivalent Chromatin Structure Marks Key Developmental Genes in Embryonic Stem Cells. *Cell.* 2006;125(2):315-26.

33. Santos-Rosa H, Schneider R, Bannister AJ, Sherriff J, Bernstein BE, Emre NC, et al. Active genes are tri-methylated at K4 of histone H3. *Nature.* 2002;419(6905):407-11.

34. Lee JH, and Skalnik DG. CpG-binding protein (CXXC finger protein 1) is a component of the mammalian Set1 histone H3-Lys4 methyltransferase complex, the analogue of the yeast Set1/COMPASS complex. *J Biol Chem.* 2005;280(50):41725-31.

35. Lee JH, Tate CM, You JS, and Skalnik DG. Identification and characterization of the human Set1B histone H3-Lys4 methyltransferase complex. *J Biol Chem.* 2007;282(18):13419-28.

36. Dou Y, Milne TA, Ruthenburg AJ, Lee S, Lee JW, Verdine GL, et al. Regulation of MLL1 H3K4 methyltransferase activity by its core components. *Nature structural & molecular biology.* 2006;13(8):713-9.

37. Mohan M, Lin C, Guest E, and Shilatifard A. Licensed to elongate: a molecular mechanism for MLL-based leukaemogenesis. *Nature reviews Cancer.* 2010;10(10):721-8.

38. Wu M, Wang PF, Lee JS, Martin-Brown S, Florens L, Washburn M, et al. Molecular regulation of H3K4 trimethylation by Wdr82, a component of human Set1/COMPASS. *Mol Cell Biol.* 2008;28(24):7337-44.

39. Lee JH, Tate CM, You JS, and Skalnik DG. Identification and characterization of the human Set1B histone H3-Lys4 methyltransferase complex. *J Biol Chem.* 2007;282(18):13419-28.

40. Lee JH, and Skalnik DG. Wdr82 is a C-terminal domain-binding protein that recruits the Setd1A Histone H3-Lys4 methyltransferase complex to transcription start sites of transcribed human genes. *Mol Cell Biol.* 2008;28(2):609-18.

41. Bi Y, Lv Z, Wang Y, Hai T, Huo R, Zhou Z, et al. WDR82, a key epigenetics-related factor, plays a crucial role in normal early embryonic development in mice. *Biol Reprod.* 2011;84(4):756-64.

42. Lee JH, You J, Dobrota E, and Skalnik DG. Identification and characterization of a novel human PP1 phosphatase complex. *J Biol Chem.* 2010;285(32):24466-76.

43. Chapman-Rothe N, Curry E, Zeller C, Liber D, Stronach E, Gabra H, et al. Chromatin H3K27me3/H3K4me3 histone marks define gene sets in high-grade serous ovarian cancer that distinguish malignant, tumour-sustaining and chemo-resistant ovarian tumour cells. *Oncogene.* 2013;32(38):4586-92.

44. Kim SS, Lee MH, and Lee MO. Histone methyltransferases regulate the transcriptional expression of ERα and the proliferation of tamoxifen-resistant breast cancer cells. *Breast Cancer Res Treat.* 2020;180(1):45-54.

45. Hasan T, Caragher SP, Shireman JM, Park CH, Atashi F, Baisiwala S, et al. Interleukin-8/CXCR2 signaling regulates therapy-induced plasticity and enhances tumorigenicity in glioblastoma. *Cell death & disease.* 2019;10(4):292.

46. Bounaix Morand du Puch C, Barbier E, Kraut A, Coute Y, Fuchs J, Buhot A, et al. TOX4 and its binding partners recognize DNA adducts generated by platinum anticancer drugs. *Arch Biochem Biophys.* 2011;507(2):296-303.

47. McDonald JW, and Pilgram TK. Nuclear expression of p53, p21 and cyclin D1 is increased in bronchioloalveolar carcinoma. *Histopathology.* 1999;34(5):439-46.

48. Dobin A, Davis CA, Schlesinger F, Drenkow J, Zaleski C, Jha S, et al. STAR: ultrafast universal RNA-seq aligner. *Bioinformatics.* 2013;29(1):15-21.

49. Anders S, Pyl PT, and Huber W. HTSeq--a Python framework to work with high-throughput sequencing data. *Bioinformatics.* 2015;31(2):166-9.

50. Love MI, Huber W, and Anders S. Moderated estimation of fold change and dispersion for RNA-seq data with DESeq2. *Genome biology.* 2014;15(12):550.

51. Langmead B, Trapnell C, Pop M, and Salzberg SL. Ultrafast and memory-efficient alignment of short DNA sequences to the human genome. *Genome biology.* 2009;10(3):R25.

52. Cawthorne C, Swindell R, Stratford IJ, Dive C, and Welman A. Comparison of doxycycline delivery methods for Tet-inducible gene expression in a subcutaneous xenograft model. *Journal of biomolecular techniques : JBT.* 2007;18(2):120-3.

53. Volm M, Koomägi R, Stammler G, Rittgen W, Zintl F, and Sauerbrey A. Prognostic implications of cyclins (D1, E, A), cyclin-dependent kinases (CDK2, CDK4) and tumor-suppressor genes (pRB, p16INK4A) in childhood acute lymphoblastic leukemia. *Int J Cancer.* 1997;74(5):508-12.

54. Franken NA, Rodermond HM, Stap J, Haveman J, and van Bree C. Clonogenic assay of cells in vitro. *Nat Protoc.* 2006;1(5):2315-9.

55. Li P, Weng Z, Li P, Hu F, Zhang Y, Guo Z, et al. BATF3 promotes malignant phenotype of colorectal cancer through the S1PR1/p-STAT3/miR-155-3p/WDR82 axis. *Cancer Gene Ther.* 2021;28(5):400-12.

56. Lei J, Chen P, Zhang F, Zhang N, Zhu J, Wang X, et al. M2 macrophages-derived exosomal microRNA-501-3p promotes the progression of lung cancer via targeting WD repeat domain 82. *Cancer Cell Int.* 2021;21(1):91.

57. An S, Camarillo JM, Huang TY, Li D, Morris JA, Zoltek MA, et al. Histone tail analysis reveals H3K36me2 and H4K16ac as epigenetic signatures of diffuse intrinsic pontine glioma. *J Exp Clin Cancer Res.* 2020;39(1):261.

58. Larson JD, Kasper LH, Paugh BS, Jin H, Wu G, Kwon CH, et al. Histone H3.3 K27M Accelerates Spontaneous Brainstem Glioma and Drives Restricted Changes in Bivalent Gene Expression. *Cancer cell.* 2019;35(1):140-55.e7.

59. Sweha SR, Chung C, Natarajan SK, Panwalkar P, Pun M, Ghali A, et al. Epigenetically defined therapeutic targeting in H3.3G34R/V high-grade gliomas. *Science translational medicine.* 2021;13(615):eabf7860.

60. Ma Q, Long W, Xing C, Jiang C, Su J, Wang HY, et al. PHF20 Promotes Glioblastoma Cell Malignancies Through a WISP1/BGN-Dependent Pathway. *Frontiers in oncology.* 2020;10:573318.

61. Dai B, Xiao Z, Zhu G, Mao B, Huang H, Guan F, et al. WD Repeat Domain 5 Promotes Invasion, Metastasis and Tumor Growth in Glioma Through Up-Regulated Zinc Finger E-Box Binding Homeobox 1 Expression. *Cancer Manag Res.* 2020;12:3223-35.

62. Wang F, Zhang J, Ke X, Peng W, Zhao G, Peng S, et al. WDR5-Myc axis promotes the progression of glioblastoma and neuroblastoma by transcriptional activating CARM1. *Biochem Biophys Res Commun.* 2020;523(3):699-706.

63. Tan Z, Chen K, Wu W, Zhou Y, Zhu J, Wu G, et al. Overexpression of HOXC10 promotes angiogenesis in human glioma via interaction with PRMT5 and upregulation of VEGFA expression. *Theranostics.* 2018;8(18):5143-58.

64. Zhou C, Zhang Y, Dai J, Zhou M, Liu M, Wang Y, et al. Pygo2 functions as a prognostic factor for glioma due to its up-regulation of H3K4me3 and promotion of MLL1/MLL2 complex recruitment. *Sci Rep.* 2016;6:22066.

65. Taylor JT, Ellison S, Pandele A, Wood S, Nathan E, Forte G, et al. Actinomycin D downregulates Sox2 and improves survival in preclinical models of recurrent glioblastoma. *Neuro-oncology.* 2020;22(9):1289-301.

66. Lopez-Bertoni H, Kotchetkov IS, Mihelson N, Lal B, Rui Y, Ames H, et al. A Sox2:miR-486-5p Axis Regulates Survival of GBM Cells by Inhibiting Tumor Suppressor Networks. *Cancer Res.* 2020;80(8):1644-55.

67. Guerra-Rebollo M, Garrido C, Sánchez-Cid L, Soler-Botija C, Meca-Cortés O, Rubio N, et al. Targeting of replicating CD133 and OCT4/SOX2 expressing glioma stem cells selects a cell population that reinitiates tumors upon release of therapeutic pressure. *Sci Rep.* 2019;9(1):9549.

68. Franks TM, McCloskey A, Shokirev MN, Benner C, Rathore A, and Hetzer MW. Nup98 recruits the Wdr82-Set1A/COMPASS complex to promoters to regulate H3K4 trimethylation in hematopoietic progenitor cells. *Genes Dev.* 2017;31(22):2222-34.

69. Zuccolo M, Alves A, Galy V, Bolhy S, Formstecher E, Racine V, et al. The human Nup107-160 nuclear pore subcomplex contributes to proper kinetochore functions. *EMBO J.* 2007;26(7):1853-64.

70. Loïodice I, Alves A, Rabut G, Van Overbeek M, Ellenberg J, Sibarita JB, et al. The entire Nup107-160 complex, including three new members, is targeted as one entity to kinetochores in mitosis. *Mol Biol Cell.* 2004;15(7):3333-44.

71. Gagrica S, Hauser S, Kolfschoten I, Osterloh L, Agami R, and Gaubatz S. Inhibition of oncogenic transformation by mammalian Lin-9, a pRB-associated protein. *EMBO J.* 2004;23(23):4627-38.

72. Esterlechner J, Reichert N, Iltzsche F, Krause M, Finkernagel F, and Gaubatz S. LIN9, a subunit of the DREAM complex, regulates mitotic gene expression and proliferation of embryonic stem cells. *PloS one.* 2013;8(5):e62882.

73. Litovchick L, Sadasivam S, Florens L, Zhu X, Swanson SK, Velmurugan S, et al. Evolutionarily conserved multisubunit RBL2/p130 and E2F4 protein complex represses human cell cycle-dependent genes in quiescence. *Mol Cell.* 2007;26(4):539-51.

74. Davis AJ, Tsinkevich M, Rodencal J, Abbas HA, Su XH, Gi YJ, et al. TAp63-Regulated miRNAs Suppress Cutaneous Squamous Cell Carcinoma through Inhibition of a Network of Cell-Cycle Genes. *Cancer Res.* 2020;80(12):2484-97.

75. Chayka O, D'Acunto CW, Middleton O, Arab M, and Sala A. Identification and pharmacological inactivation of the MYCN gene network as a therapeutic strategy for neuroblastic tumor cells. *J Biol Chem.* 2015;290(4):2198-212.

76. Tassinari V, Cesarini V, Tomaselli S, Ianniello Z, Silvestris DA, Ginistrelli LC, et al. ADAR1 is a new target of METTL3 and plays a pro-oncogenic role in glioblastoma by an editing-independent mechanism. *Genome biology.* 2021;22(1):51.

77. Bolin S, Borgenvik A, Persson CU, Sundström A, Qi J, Bradner JE, et al. Combined BET bromodomain and CDK2 inhibition in MYC-driven medulloblastoma. *Oncogene.* 2018;37(21):2850-62.

78. Min C, Yu Z, Kirsch KH, Zhao Y, Vora SR, Trackman PC, et al. A loss-of-function polymorphism in the propeptide domain of the LOX gene and breast cancer. *Cancer Res.* 2009;69(16):6685-93.

79. Bouez C, Reynaud C, Noblesse E, Thépot A, Gleyzal C, Kanitakis J, et al. The lysyl oxidase LOX is absent in basal and squamous cell carcinomas and its knockdown induces an invading phenotype in a skin equivalent model. *Clin Cancer Res.* 2006;12(5):1463-9.

80. Gasset-Rosa F, Lu S, Yu H, Chen C, Melamed Z, Guo L, et al. Cytoplasmic TDP-43 De-mixing Independent of Stress Granules Drives Inhibition of Nuclear Import, Loss of Nuclear TDP-43, and Cell Death. *Neuron.* 2019;102(2):339-57.e7.

81. Hazawa M, Lin DC, Kobayashi A, Jiang YY, Xu L, Dewi FRP, et al. ROCK-dependent phosphorylation of NUP62 regulates p63 nuclear transport and squamous cell carcinoma proliferation. *EMBO reports.* 2018;19(1):73-88.

82. Ali A, Veeranki SN, and Tyagi S. A SET-domain-independent role of WRAD complex in cell-cycle regulatory function of mixed lineage leukemia. *Nucleic Acids Res.* 2014;42(12):7611-24.

83. Tajima K, Yae T, Javaid S, Tam O, Comaills V, Morris R, et al. SETD1A modulates cell cycle progression through a miRNA network that regulates p53 target genes. *Nat Commun.* 2015;6:8257.

84. Morel AP, Sentis S, Bianchin C, Le Romancer M, Jonard L, Rostan MC, et al. BTG2 antiproliferative protein interacts with the human CCR4 complex existing in vivo in three cell-cycle-regulated forms. *J Cell Sci.* 2003;116(Pt 14):2929-36.

Figure legends

Figure 1. H3K4me3 is associated with malignancy and prognosis of pediatric gliomas. A. Immunohistochemistry (IHC) shows H3K4me3 in WHO grade I-IV pediatric gliomas. B. Quantitative IHC results for H3K4me3 in pediatric gliomas. C. Survival analysis of pediatric gliomas based on H3K4me3 IHC results. D. Expressions of WDR82, SETD1A and H3K4me3 detected with western blots in fresh pediatric glioma specimens. Abbreviations: PA, pilocytic astrocytoma; DA, diffuse astrocytoma; PXA, pleomorphic xanthoastrocytoma; AA, anaplastic astrocytoma; GBM, glioblastoma.

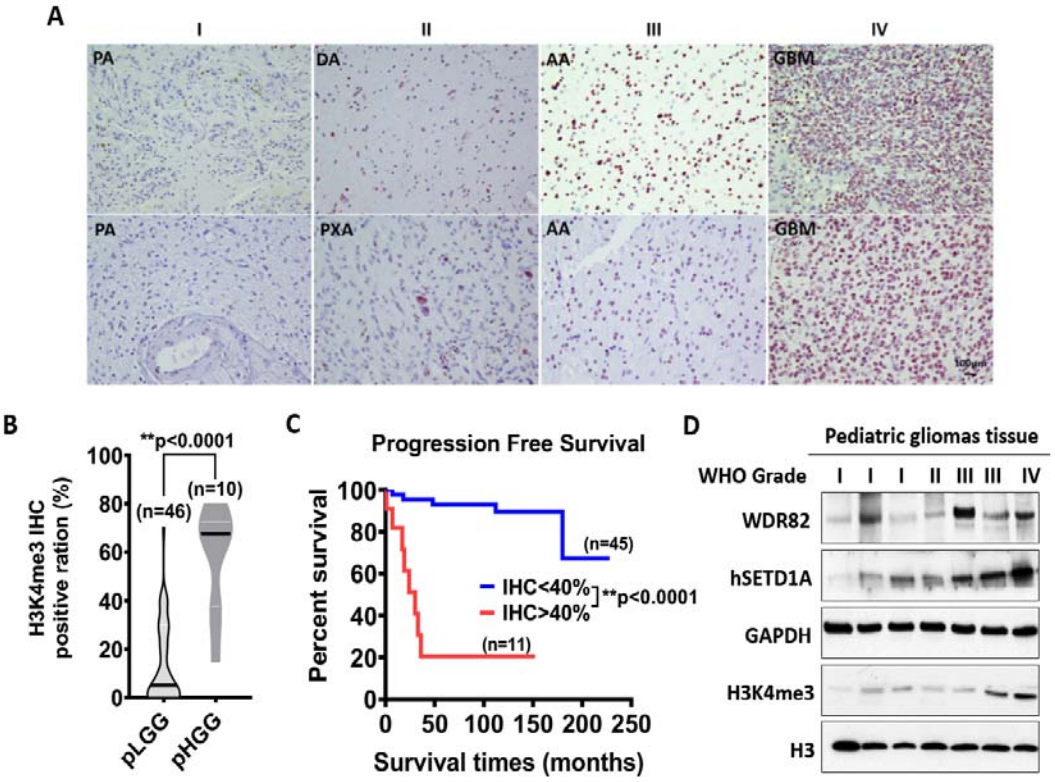

Figure 2. WDR82 is associated with malignancy in pediatric gliomas. A. WDR82 expression in WHO low- and high- grade pediatric gliomas. **B**. WDR82 expression in molecular subtypes of pediatric high-grade gliomas (pHGGs). C. In silico analysis shows WDR82 function in pediatric gliomas. D. Survival analysis of pHGGs based on WDR82 expression levels. E and F. In silico analysis of TCGA database shows WDR82 expression in adult WHO grade gliomas and survival analysis of adult gliomas based on WDR82 expression.

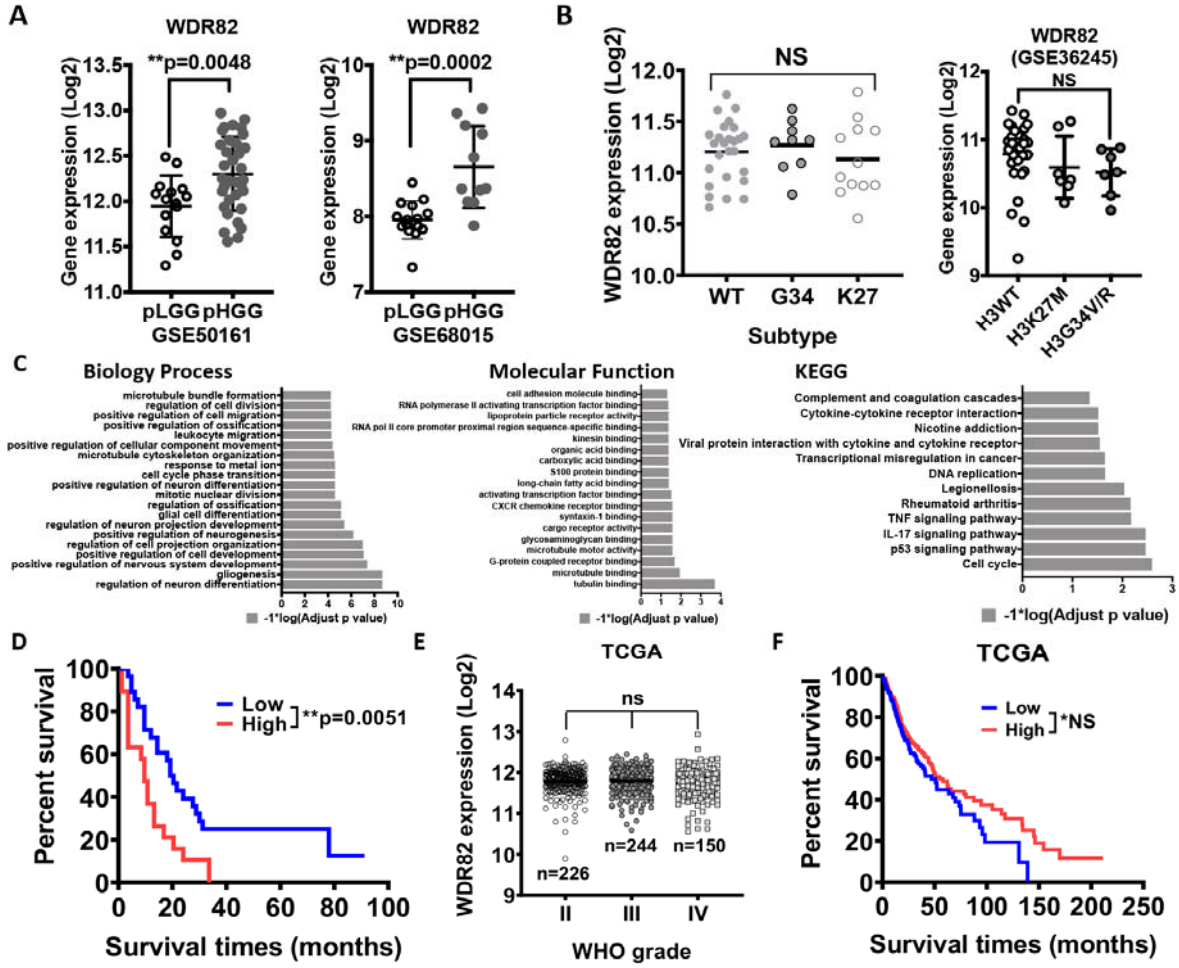

Figure 3. Establishment and validation of a WDR82 expression inducible knockdown system. A. The illustration indicates the main components of DOX inducible small hairpin WDR82 (shWDR82) lentiviral vectors. B. Representative images show SJ-GBM2, SF8628 and KNS42 cells transduced with non-target (shNT, negative control) or small hairpin RNAs (shRNA#1 and (shRNA#2) against WDR82 in the absence or presence of 2μg/ml Dox at day 5. Real-time PCR (**C**) and western blot (**D**) results using RNA and protein from cells in B.

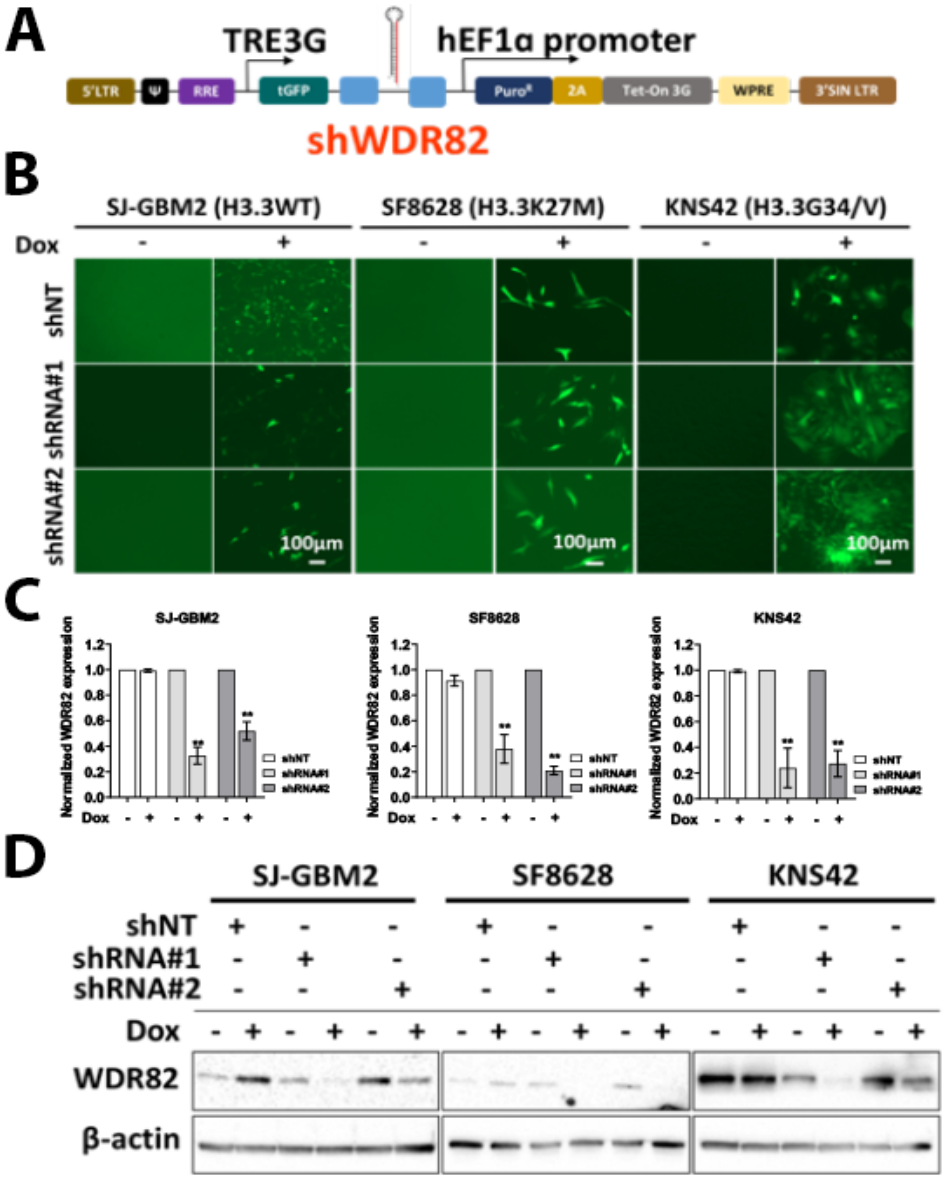

Figure 4. Altered gene expression following WDR82 inducible knockdown in pediatric SJ-GBM2 glioma cells. A. Venn diagram shows differentially expressed genes from RNA-seq results, generated from total RNA extracted from shWDR82 transduced SJ-GBM2 cells in the presence (+) and absence (-) of doxycycline. **B and C.** The heat map showed 129 differential expressed genes (B) and the top 30 genes for which expression increased or decreased in A. **D.** Gene Ontology Molecular function analysis for the top down- or upregulated genes and their associated functions. **E**. An example from ChIP-seq results shows decreased promoter H3K4me3 levels in the LIN9 and NUP43 genes following Dox induction.

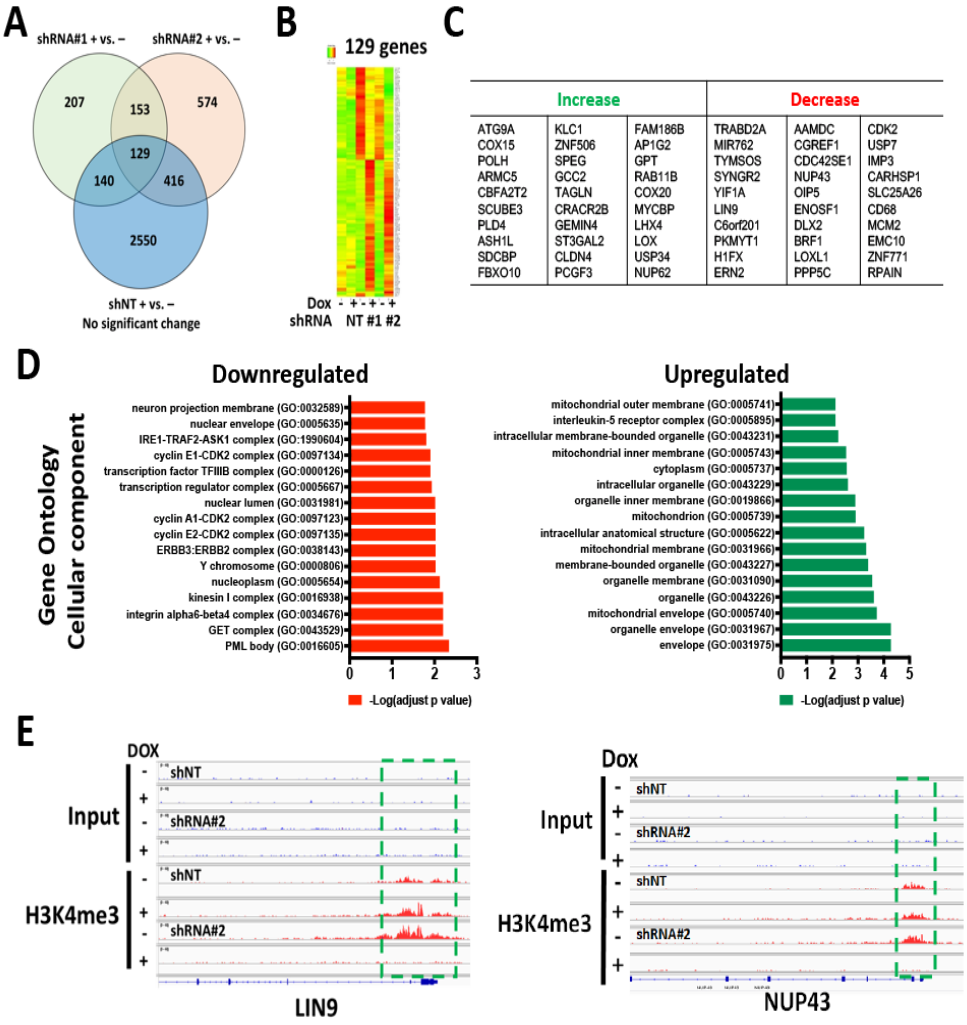

Figure 5. WDR82 regulates expression of mitotic and DNA damage repair genes through mediation of H3K4me3. A and B. Representative dot plots show genes that are not associated with WDR82 in pediatric glioma tissue specimens (**A**), for these genes H3K4me3 levels at the promoter are not altered as shown by ChIP-seq results (**B**) from SJ-GBM2 cells, treated with Dox inducible shRNA against WDR82 , in the absence and presence of Dox. **C and D.** Representative dot plots showing genes that are associated with WDR82 in pediatric glioma tissue specimens (**C**) for these genes, i.e. PKMYTI, H3K4me3 promoter levels decreased as shown with ChIP-seq results (**D**) from SJ-GBM2 cells, treated with Dox inducible shRNA against WDR82, in the absence and presence of Dox.

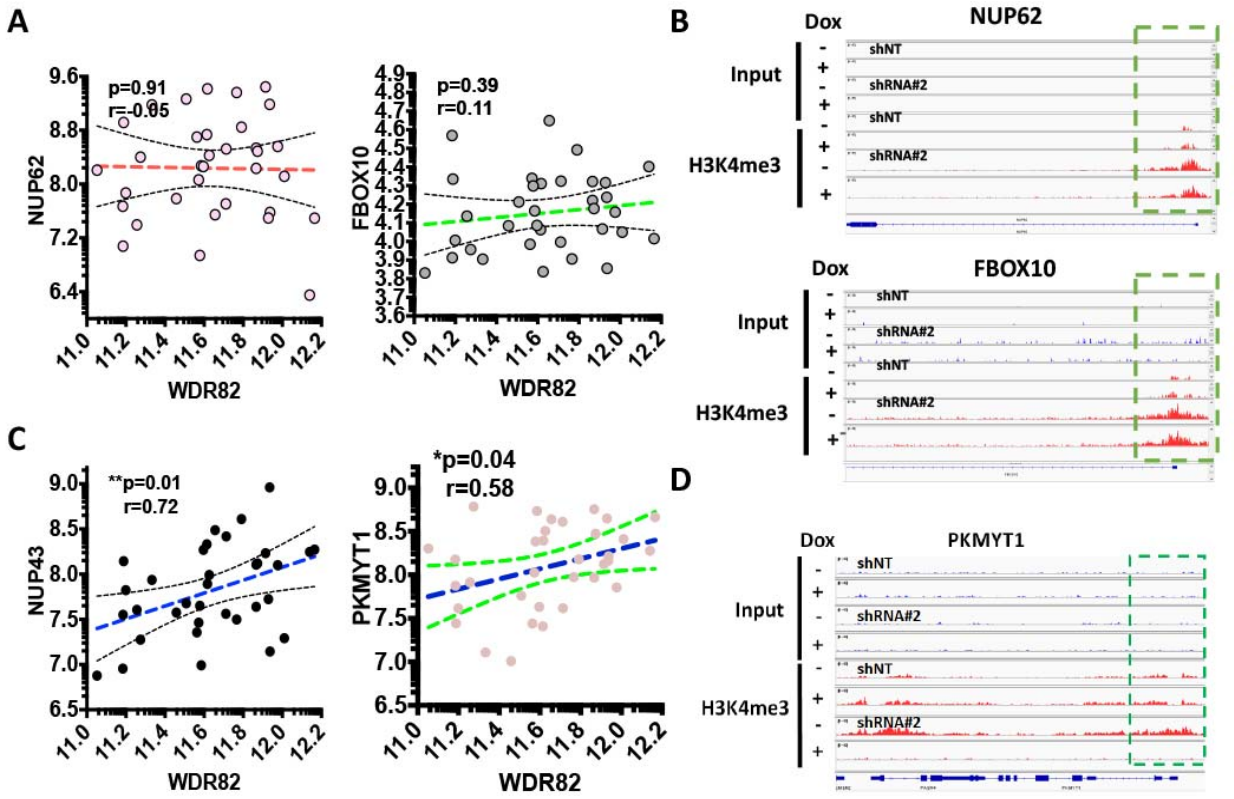

Figure 6. WDR82 knockdown decreases in vitro cell viability and proliferation and extends survival of pHGG tumor bearing mice. A. Normalized cell viability of SJ-GBM2 and SF8628 cells transduced with inducible shRNA #1 or #2 against WDR82 or non-target shRNA (shNT) in the absence or presence of Dox (2µg/ml), in comparison to parental non-treated cells. **B and C**. Representative images (**B**) and quantitative results (**C**) showed colony formation in 500 KNS42 cells transduced with shRNAs #1 or #2, or shNT in the absence or presence of Dox (2µg/ml). **D.** Correlations between WDR82 and CDK2 in pediatric gliomas. **E.** ChIPseq results for H3K4me3 levels at CDK2 and CCND1 promoters in the absence and presence of Dox in SJ-GBM2 cells. **F.** The illustration indicates WDR82 mediated H3K4me3 at CCND1 promoter regulates cell proliferation, cell cycle and DNA damage through activating the cyclin D1-CDK2 signaling pathway.

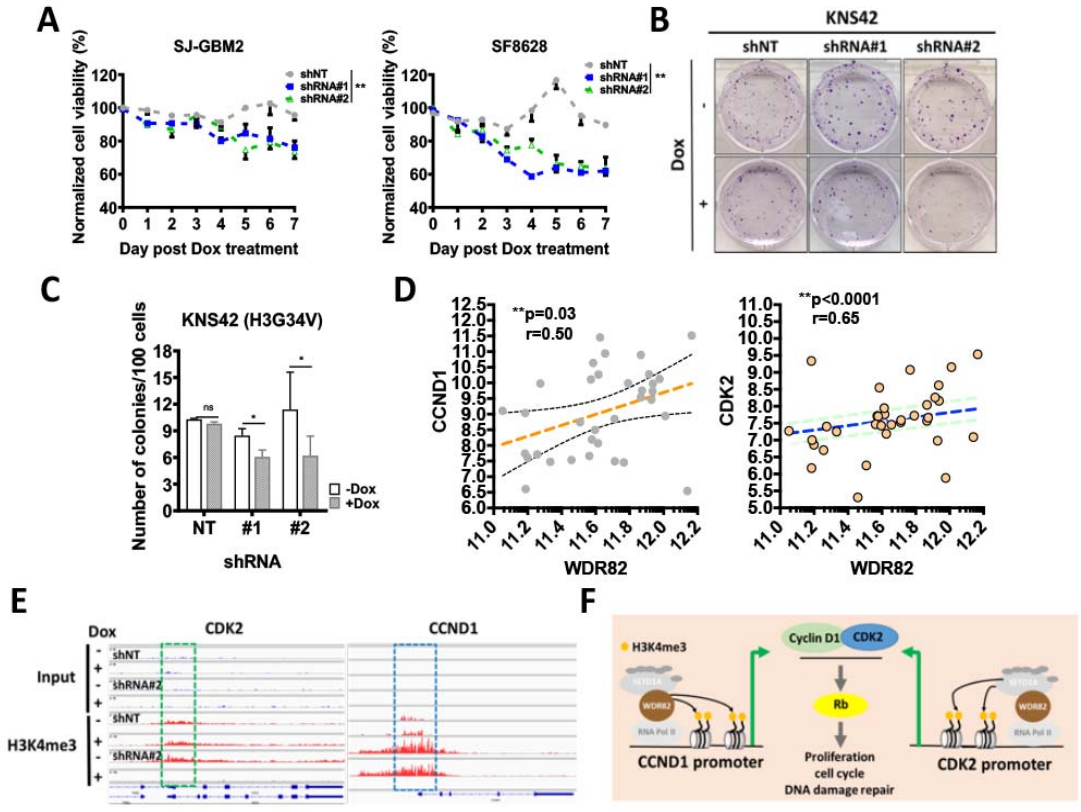

Figure 7. WDR82 and H3K4me3 are associated with cell proliferation; WDR82 knockdown decreases in vivo pHGG tumor growth and extends survival of pHGG tumor bearing mice. A. Correlation between PCNA, MIK67 and WDR82 in pediatric glioma tissue specimens. **B.** Representative immunohistochemistry staining shows Ki67 and H3K4me3 in pediatric astrocytoma (PA, WHO grade I, GrI) and glioblastoma (GBM, WHO grade IV, GrIV) tumor samples. **C.** Representative HE images show tumors in shNT and shRNA#2 treated cells with or without Dox (2mg/ml). **D and E**. Mitotic cells in HE stained slides (**D**) and relative quantification per high power field (400x) (**E**) from in vivo intracranial SJ-GBM2 xenograft tumors with or without Dox induction. **F.** Survival curve for mice inoculated with SJ-GBM2 cells transduced with shNT and shRNA#2 against WDR82 with or without Dox.